Since January 2020 Elsevier has created a COVID-19 resource centre with free information in English and Mandarin on the novel coronavirus COVID-19. The COVID-19 resource centre is hosted on Elsevier Connect, the company's public news and information website.

Journal of Theoretical Biology 542 (2022) 111109

Contents lists available at ScienceDirect

Journal of Theoretical Biology

journal homepage: www.elsevier.com/locate/yjtbi

Contact tracing-induced Allee effect in disease dynamics

Matías Arim [a,b,1,*], Daniel Herrera-Esposito [b,c], Paola Bermolen [b,d], Álvaro Cabana [b,e], María Inés Fariello [b,d], Mauricio Lima [f,g], Hector Romero [a,b,h,1]

[a] Departamento de Ecología y Gestión Ambiental, Centro Universitario Regional Este (CURE), Universidad de la República, Uruguay
[b] CICADA, Centro Interdisciplinario de Ciencia de Datos y Aprendizaje Automático, Universidad de la República, Uruguay
[c] Laboratorio de Neurociencias, Instituto de Biología, Facultad de Ciencias, Universidad de la República, Uruguay
[d] Instituto de Matemática y Estadística Rafael Laguardia, Facultad de Ingeniería, Universidad de la República, Uruguay
[e] Center for Basic Research in Psychology (CIBPsi) & Instituto de Fundamentos y Métodos, Facultad de Psicología, Universidad de la República, Uruguay
[f] Departamento de Ecología, Pontificia Universidad Católica de Chile, Santiago, Chile
[g] Center of Applied Ecology and Sustainability (CAPES), Pontificia Universidad Católica de Chile, Santiago, Chile
[h] Laboratorio de Genómica Evolutiva, Dpto. de Biología Celular y Molecular, Instituto de Biología, Facultad de Ciencias, Universidad de la República, Uruguay

ARTICLE INFO

Article history:
Received 6 July 2021
Revised 22 March 2022
Accepted 24 March 2022
Available online 26 March 2022

Keywords:
SARS
Allee effect
Non-pharmaceutical interventions
Outbreak threshold
Alternative states
Super-spreading
Super-spreader
TEst-TRace-ISolate
TETRIS

ABSTRACT

Contact tracing, case isolation, quarantine, social distancing, and other non-pharmaceutical interventions (NPIs) have been a cornerstone in managing the COVID-19 pandemic. However, their effects on disease dynamics are not fully understood. Saturation of contact tracing caused by the increase of infected individuals has been recognized as a crucial variable by healthcare systems worldwide. Here, we model this saturation process with a mechanistic and a phenomenological model and show that it induces an Allee effect which could determine an infection threshold between two alternative states—containment and outbreak. This transition was considered elsewhere as a response to the strength of NPIs, but here we show that they may be also determined by the number of infected individuals. As a consequence, timing of NPIs implementation and relaxation after containment is critical to their effectiveness. Containment strategies such as vaccination or mobility restriction may interact with contact tracing-induced Allee effect. Each strategy in isolation tends to show diminishing returns, with a less than proportional effect of the intervention on disease containment. However, when combined, their suppressing potential is enhanced. Relaxation of NPIs after disease containment--e.g. because vaccination--have to be performed in attention to avoid crossing the infection threshold required to a novel outbreak. The recognition of a contact tracing-induced Allee effect, its interaction with other NPIs and vaccination, and the existence of tipping points contributes to the understanding of several features of disease dynamics and its response to containment interventions. This knowledge may be of relevance for explaining the dynamics of diseases in different regions and, more importantly, as input for guiding the use of NPIs, vaccination campaigns, and its combination for the management of epidemic outbreaks.

1. Introduction

Non-pharmaceutical interventions (NPIs) such as testing, contact tracing and isolation (TETRIS), social distancing, and face masks have been applied with unprecedented strength and breadth in managing the COVID-19 pandemic (Flaxman et al., 2020; Hellewell et al., 2020; Li et al., 2020; Maier and Brockmann, 2020; Peak et al., 2017; Peak et al., 2020; Walker et al., 2020b). As a general rule, both observed dynamics and model projections indicate that the implementation of strong NPIs significantly reduced the total number of infections compared with uncontained outbreaks (Dehning et al., 2020; Flaxman et al., 2020; Hsiang et al., 2020; Li et al., 2020; Maier and Brockmann, 2020; Giordano et al., 2021; Yang et al., 2021). The effectiveness of NPIs may determine two alternative states: one of disease containment ($R_e < 1$) and another of disease outbreak ($R_e > 1$) (Ferretti et al., 2020; Flaxman et al., 2020; Hellewell et al., 2020; Siegenfeld et al., 2020). Contact tracing in particular is likely to have significant impact at low infection numbers (Hellewell et al., 2020; Klinkenberg et al., 2006), but its effect on disease transmission fades away if the epidemic increases largely surpassing contact tracing capacities (Hellewell et al., 2020; Klinkenberg et al., 2006). This is because the larger the number of infections, the lower the probability of testing all infected individu-

* Corresponding author at: Departamento de Ecología y Gestión Ambiental, Centro Universitario Regional Este (CURE), Universidad de la República, Uruguay.
E-mail address: matiasarim@gmail.com (M. Arim).
[1] Equal authorship.

https://doi.org/10.1016/j.jtbi.2022.111109
0022-5193/

als, tracking all their contacts, and notifying all contacts for quarantine (Hellewell et al., 2020; Klinkenberg et al., 2006). The fate of some countries containing COVID-19, and also Ebola, was related with the performance of their tracing systems (Lewis, 2020). Countries such as Vietnam, South Korea and Japan scaled tracing capacities to unprecedented levels being able to efficiently handle large outbreaks (Lewis, 2020). On the other hand, evidence suggesting a poor performance of contact tracing was presented for the USA or UK (Lewis, 2020). Beside these extreme scenarios, it is clear that contact tracing reduces transmission rate, that its performance depends on infection numbers, and that it interacts with other NPIs, determining a complex and poorly understood relationship with epidemic dynamics (Block et al., 2020; Chowell and Nishiura, 2014; Hellewell et al., 2020; Hsiang et al., 2020; Klinkenberg et al., 2006; Maier and Brockmann, 2020; Moore et al., 2021; Peak et al., 2017; Peak et al., 2020; Walker et al., 2020b; Yang et al., 2021).

Here we focus on the positive feedback induced by the saturation of contact tracing capacities and its interactions with other NPIs, which has critical consequences in disease dynamics, particularly at low numbers. This feedback loop connects the saturation of contact tracing with the Allee effect, a central concept in population biology characterized by the positive feedback between population abundance and population growth rate at low numbers (Berryman, 1999; Courchamp et al., 1999; Keeling and Rohani, 2011). A strong Allee effect can determine a transition from negative to positive growth rate at a given abundance threshold (Courchamp et al., 1999). In disease dynamics, this is interpreted as an epidemic breakpoint, a tipping point below which the outbreak tends to diminish ($R_e < 1$), but above which the outbreak grows ($R_e > 1$) (Alonso et al., 2019). However, this phenomenon is not captured in the many variants of SIR and logistic models widely used for the analysis, forecasting and managing of COVID-19 and other emergent diseases dynamics (Bjørnstad, 2018; Dehning et al., 2020; Flaxman et al., 2020; Hsiang et al., 2020; Li et al., 2020; Maier and Brockmann, 2020; Wu et al., 2020). We contribute to filling this gap by formalizing the connection between saturating contact tracing capacities, the strength of other NPIs, and disease dynamics. We mechanistically connect the saturation of contact tracing capacities with an Allee effect, from which abrupt transitions in growth rate are expected after a threshold in the number of infected individuals is crossed. We also include the interaction of our model with vaccination levels. A consequence of the infection threshold is that the vaccination level for disease containment is significantly reduced when combined with a strong TETRIS system and reinforced with additional NPIs as transmission barriers or reduction in mobility.

2. Methods

We analyzed the effect of saturation of contact tracing capacities with two complementary models. The first model shows a mechanistic connection between contact tracing, its saturation with the rise in infection number, and the emergence of a positive feedback in disease growth rate--an Allee effect. The second one incorporates this positive feedback in a SIR model in which transmision and recovery rate depend on infection number. The first model focuses on specific mechanisms that can generate the positive feedback between infections and growth rate, while the second model focuses on the consequences of this feedback without making its mechanisms explicit. Consequently we refer to these models as mechanistic and phenomenological respectively.

2.1. Mechanistic effect of saturation in contact tracing on reproduction number

To analyze the effect of contact tracing saturation on the epidemic reproductive ratio (R_e), we introduce a model focused on the forward tracing of contacts of detected infections (Klinkenberg et al., 2006). This model attempts to explicitly account for the main steps of the contact tracing system: detecting infections, tracing contacts, and isolating individuals to stop transmissions. We focus on the timing of these events and its consequence for disease transmission. In this sense, this model provides a mechanistic connection between the contact tracing system and the Allee effect.

First, we define R_e^{nq} (nq: non quarantine) as the reproductive number (or average number of secondary infections) of individuals in the absence of contact tracing and quarantine. For clarity, we use the term quarantine to refer to both 'quarantine' and 'case isolation'. The value of R_e^{nq} is determined by the number of social links accumulated during the infectious period (L_{max}), the probability of disease transmission in each link (b_{link}), and the probability of having a link with a susceptible individual ($P_{susceptible}$= (*N-I-R-1*)/(*N-1*), with N being population size and I and R the infected and recovered individuals respectively) thus $R_e^{nq} = P_{susceptible} \cdot b_{link} \cdot L_{max}$ (Fig. 1A). While the value of b_{link} is reduced by the use of face masks, hygienic measures, and physical distancing (Prather et al., 2020), the number of social links L_{max} can be reduced through contact tracing and subsequent quarantine (Hellewell et al., 2020; Lewis, 2020). How much it can be reduced depends on how many days after infection the individual is detected and quarantined which depends on the contact tracing system capacity. To model the limited capacity of the contact tracing and how it affects the number of social links generated during the infection period, we introduce a maximum number of cases (K) that can be detected by the test and trace system in a day. Furthermore, following the classical consumer-victim literature (Gotelli, 2008), we model the fraction of infected individuals that are detected (f_q) as a Type II functional response of the number of infected individuals by the equation $f_q = K/(I_{50,D} + I)$, where $I_{50,D}$ is the number of infected cases at which half the maximum detection capacity is reached. As f_q cannot be >1, we further considered that $f_q = \min(1, K/(I_{50,D} + I))$. This also leads to a total number of detected individuals given by $D = f_q \cdot I$. The value of $I_{50,D}$ in contact tracing is proportional to the inverse of the detection efficiency of an infected individual times the handling time of each infected one (see Gotelli, 2008 pp136). The total handling time of a case is determined by the time associated with testing, interviews to find out who was exposed and calling or visiting those exposed individuals to tell them they need to quarantine (Lewis, 2020). Further, the maximum number of cases that can be detected (K) is the inverse of the handling time of each case times the number of tracers. Consequently, the type II functional response could be derived from the contact tracing capacities and explicitly connects main--and quantifiable--features of the tracing system and its saturation with the rise in the number of infections.

We also consider the effect that the increase in contact tracing demand has in the time lag between infection and detection, and how this affects secondary infections. For clarity, we refer to infection by the day of exposure not the day of becoming infectious. For this, we first introduce a fixed number of calls (or visits) that can be done by the tracing system each day to locate the detected individuals (N_{calls}), each with a probability (P_{find}) of finding the individual. Consequently, the expected number of calls made per detected individual on a given day is N_{calls}/D, which could be >1 (when the system has idle capacity), and the probability of finding and quarantining an infected individual is $P_q = 1-(1-P_{find})^{Ncalls/D}$. Thus, assuming that individuals can be traced immediately after getting infected, the probability that an individual is contacted and quarantined on day d after the date of infection (isolation delay) follows the geometric distribution $P(d) = P_q(1-P_q)^{d-1}$. Note that this probability decreases when d increases. Also, we assume that during this period individuals establish social links with infectious potential

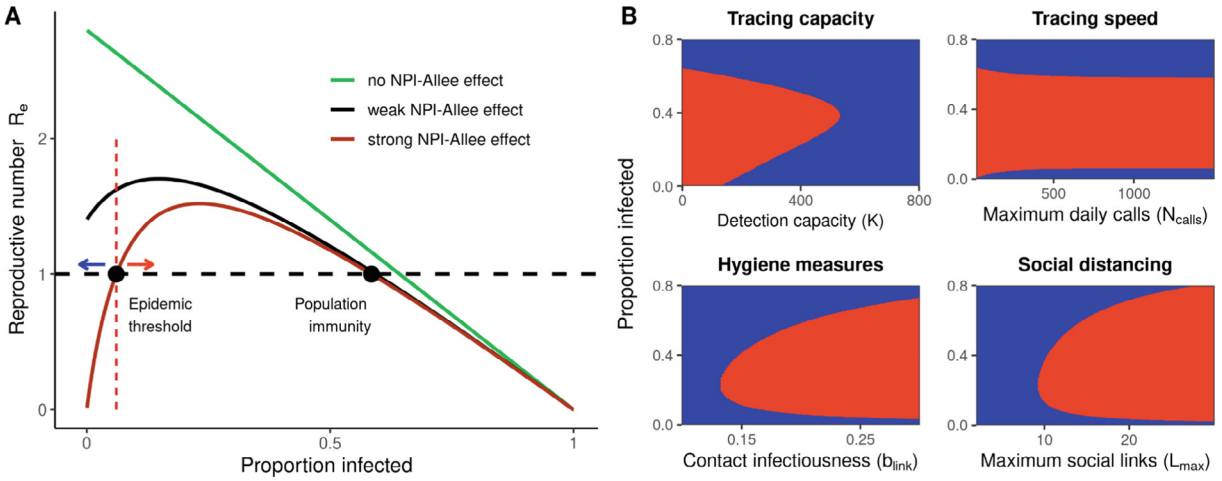

Fig. 1. Saturation of contact tracing and disease dynamics. **(A)** Effective reproduction number as a function of the proportion of the population infected $R_e(I)$. Without contact tracing (green line) the per capita growth rate $R_e(I)$ decreases proportionally to I indicating a logistic dynamics. When contact tracing is in place (red and black lines) $R_e(I)$ first increases with the proportion of infected individuals due to the saturation of the tracing system inducing an Allee effect (Eq. (1)). When the Allee effect is strong an epidemic threshold at low numbers is observed. Arrows highlight the expected trend in infection numbers around the infection threshold. This figure presents an initial state of the epidemic in which the number of recovered individuals is zero. The growth in recovery numbers–or the advance in immunization–translate these curves to lower reproductive numbers–reducing the red area in B (e.g. Fig. 3B). For the green line with no NPI, the detection capacity in the model is set to 0, removing the effect of tracing. For the red line with strong NPI-Allee effect, the model parameters are P_{find} = 0.1, N_{Calls} = 800, b_{link} = 0.2, L_{Max} = 14, K = 200 and I_{50} = 200. For the black line showing weak NPI-Allee effect, the model parameters are the same as for the strong NPI-Allee effect, except for I_{50} which is set to 400. All examples use a total population size N of 2000 individuals. (**B**) The alternative epidemic states of growth ($R_e(I) > 1$, red) or containment ($R_e(I) < 1$, blue) are determined by both the proportion of the infected population (vertical axis) and the strength of the different NPIs (horizontal axis). All parameters are fixed to the same values as the strong NPI-Allee effect in panel **(A)**, with the exception of the parameter whose value was varied (indicated in the horizontal axis).

according to the function $L(d) = L_{max} \cdot d^4/(d^4 + 7^4)$ (see He et al., 2020) and that the infection potential vanishes when the individuals are isolated. This function assumes a humped distribution in the number of social links with infection potential with a maximum on the seventh day after infection, when accumulated social links reach half its maximum value ($L_{max}/2$). This function accounts for the rise and decay in virus load after infection (see He et al., 2020). The increase in accumulated social links with time together with the distribution of quarantine delays determines the expected number of social links that an individual generates before quarantine: $L = \Sigma_{d \geq 1} P(d) \cdot L(d)$ in contrast with L_{max} links generated by non quarantined individuals. Thus the effective reproductive number of a quarantined individual is $R_e^q = P_{susceptible} \cdot b_{link} \cdot L$.

Finally, we can express the effective reproduction number in a population with limited contact tracing as a function of the number of infected individuals, $R_e(I)$, by adding the mean secondary infections of quarantined (f_q) and non quarantined (f_{nq}) infected individuals, ponderated by their respective probabilities, as:

$$R_e(I) = R_e^q f_q + R_e^{nq} f_{nq} = P_{susceptible}\, b_{link} (L f_q + L_{\max} f_{nq}) \quad (1)$$

This formulation assumes that:

i. there is a maximum number of cases that can be processed in a day by the contact tracing system.
ii. the number of cases effectively detected follow a type II functional response.
iii. infected individuals are detected by the tracing system on the day in which they were infected. At this moment starts the effort to contact and isolate these individuals.
iv. transmission has a maximum seven days after the infection, modeling the accumulation of social links with infectious potential with a sigmoidal function.
v. the time frame of link accumulation is smaller than the time interval between infection and second infections.
vi. the contact and isolation of one individual stops transmission.
vii. infected cases not detected in a day will not be detected in the future.
viii. information about contacts is immediately available to tracers.

Note that the main messages of this model should not be affected by changes in assumptions such as the shape of functional response, the delay in infection and detection, or the rate of social link accumulation, insofar as a maximum tracing capacity and accumulation of social links through time persist. Similarly, deviations from other assumptions are expected to reinforce the saturation of the contact tracing system and the strength of the Allee effect—i.e. positive feedback loop at low numbers.

The interaction between contact tracing and vaccination was also analyzed for this model. Vaccination affects the probability of having a link with a susceptible individual, which now has to also be a non immunized individual. Adding this non-vaccinated probability in Eq. (1) ($R_e(I) = P_{non\text{-}vaccinated|susceptible} \cdot P_{susceptible} \cdot b_{link} \cdot (L \cdot f_q + L_{max} \cdot f_{nq})$) allows us to explore the effect of vaccination on epidemic containment under different scenarios of contact tracing capacities, social links--e.g. mobility--and adherence to face masks and other physical distancing measures. We modelled vaccination as 100% effective and consequently that all infected individuals were not vaccinated. However, it should be noted that the efficiency of vaccination for stopping transmission could explicitly be included in a similar way adding a "non effective vaccination probability". In our analysis, the non-vaccinated probability may be considered as the combined fraction of real non-vaccinated individuals and the fraction of the population in which vaccination did not elicit a fully protective immune response. The interaction between vaccination and contact tracing capacities was explored considering a gradient in the maximum number of cases that can be detected in a day (K). The parameter I50 was equal to K for these analyses. In addition, the interaction with other NPIs was evaluated considering different levels of social links (L_{max}) and probability of disease transmission in each link (b_{link}). For each combination

of parameters we retain a "vaccination threshold", which is the fraction of individuals vaccinated in the population such that Re < 1 for all values of I.

2.2. Model of disease dynamics with limited contact tracing

The saturation of contact tracing is translated into an increase in the transmission rate and the duration of the infection period. Here we assume that both, the rate of disease transmission, β, and the average duration of the infection period, τ, grow with the number of infected individuals $I(t)$, following the saturating functions $\beta_t(I) = \beta_0+(\beta_{max}-\beta_0)\cdot I(t)/(I_{50.\beta} + I(t))$ and $\tau_t(I) = \tau_0+(\tau_{max}-\tau_0)\cdot I(t)/(I_{50.\tau} + I(t))$ respectively (Fig. A.1). These functions capture the saturation mechanisms considered in the previous model, but are not limited to this specific scenario, accounting for several ones in which containment capacity decreases with infection number (e.g. Abdelrazec et al. 2016; Chowell and Nishiura, 2014; Gumel, 2012). The parameters $I_{50.\beta}$ and $I_{50.\tau}$ are the number of infections at which transmission rate and infection period attain half of its maximum values β_{max} and τ_{max}. β_0 and τ_0 represent the smaller transmission rate and infection period, which are attained at the lower level of infection. The better the performance of a tracing system is, the larger the $I_{50.\beta}$ and $I_{50.\tau}$ will be. These parameters resume the different components of the tracing strategy. The dynamics of the model then obey the following formulas:

$$dS/dt = -\beta_t(I)IS/N \quad (2)$$

$$dI/dt = \beta_t(I)I\,S/N - I/\tau(I)$$

$$dR/dt = I/\tau(I)$$

The effective reproductive number in this model is determined by $Re = \beta(I)\cdot(S/N)\cdot\tau(I)$. Following the logic of the previous model, we estimated the association between Re and I, as well as, its dependence on the parameters β_{max}, $I_{50.\beta}$, β_0, τ_{max}, $I_{50.\tau}$, and τ_0. These parameters capture the saturation in contact tracing ($I_{50.\beta}$, $I_{50.\tau}$), the strength of other NPIs (β_{max}, τ_{max}) and the maximum effect of the intervention (β_0 and τ_0). Nevertheless, an explicit account for the mechanisms determining these variations is not included. In this vein, is important to note that this model represents more generally any process in which the transmission rate or the duration of the infectious period increases with I: a phenomenon expected in different epidemiological scenarios (e.g. Alonso et al., 2019; Chowell and Nishiura, 2014; Gumel, 2012).

3. Results

In Fig. 1, we show the relation between the effective reproductive number of the disease—per capita growth rate—and the proportion of individuals infected at a given time, as obtained from the mechanistic model of the effect of saturation on contact tracing. These plots present an initial state of the epidemic in which a fraction of the population was infected and thus there are no individuals in the population who recovered from the disease.

In the absence of contact tracing the effective reproductive number of the disease proportionally decreases with the number of infections (Fig. 1A). This is the basic logistic dynamic (Gotelli, 2008), which supports the use of logistic models to forecast infection dynamics in different diseases (Chowell et al., 2019; Roosa et al., 2020; Viboud et al., 2016). However, when contact tracing is implemented, the effective reproductive number is reduced and a positive relationship between the infected individuals in a population and the epidemic reproduction is expected, conforming an Allee effect (Berryman, 1999; Courchamp et al., 1999). In particular, when contact tracing is strong enough, it is expected that the epidemic does not take off at low infection numbers ($R_e(I) < 1$), requiring a minimum level of infections (I^*) to cause an outbreak ($R_e(I) > 1$). The magnitude of the contact tracing response (K, Ncalls, see methods) has a nonlinear relationship with outbreak threshold I^* (Fig. 1B, upper row). In addition, interactions with other NPIs as transmission barriers and social distancing (b_{link} and L_{max} respectively, see methods) also produce a nonlinear relationship when interacting with a saturating model of contact tracing (Fig. 1B, lower row). Alternative states of growing or diminishing dynamics were considered elsewhere for COVID-19 and other diseases as a response to the strength of NPIs (Ferretti et al., 2020; Flaxman et al., 2020; Hellewell et al., 2020; Siegenfeld et al., 2020; Grantz et al. 2021). Here, we show that the transition from containment to outbreak (i.e. $R_e(I) < 1 \Rightarrow R_e(I) > 1$) may be also determined by the number of infected individuals (Fig. 1A and B).

The same messages about the emergence of an Allee effect and its dynamic consequences are obtained when the saturation mechanism is included in a general SIR model (Fig. 2). The saturation of the contact tracing at high infection numbers (large $I_{50.\beta}$ and $I_{50.\tau}$) or strong implementations of other NPIs as transmission barriers and reduction in social interactions (represented by the β_{max}) or self isolation (τ_{max}), may determine alternative states of growing or diminishing dynamics. However, alternative states are also determined by the number of infected individuals (Figs. 1 and 2). Figs. 1 and 2 may appear redundant; however, it is the consistency in the messages obtained by the two complementary approaches that has to be highlighted. Both, the mechanistic derivation of the effect of contact tracing on Re and the phenomenological derivation proposed in the SIR model, show that the infection outbreak depends not only on the strength of interventions, but also, on the level of infection attained in the population. In addition, both approaches indicate that the infection threshold and the population immunity present nonlinear interactions with other NPIs.

Contact tracing systematically reduces the fraction of the population that has to be vaccinated to ensure epidemic containment (Fig. 3). Further, a nonlinear relationship was observed with a steep decrease in the required vaccination level to revert epidemic growth rate when contact tracing and other NPIs are implemented. The tracing strategy was found to interact with other NPIs, suggesting that a strong contact tracing system, jointly with transmission barriers and reduction in mobility may promote the containment of the epidemic at significantly lower levels of vaccination than those required when vaccination is not combined with a set of NPIs.

4. Discussion

NPIs have been historically used for the management of epidemics. However, the need for a much better understanding of its connections with disease dynamics, and with other type of interventions, was repeatedly claimed (Hellewell et al., 2020; Klinkenberg et al., 2006; Lee et al., 2012; Markel et al., 2007; Moore et al., 2021; Peak et al., 2017; Peak et al., 2020; Yang et al., 2021). Here we focus on contact tracing and its dependence on the number of infections (I), their interaction with other NPIs and vaccination, and their effect on disease dynamics. In particular, we formally connect the saturation of tracing capacities with the emergence of a positive feedback in disease growth rate that conforms to an Allee effect. The modelling framework herein presented considers explicitly the synergistic effects of the contact tracing system, alternative containment interventions, and vaccination (Moore et al., 2021; Peak et al., 2020; Yang et al., 2021). Distancing interventions are represented by the parameter L_{max}—social interactions—, barriers to transmission by the parameter b_{link} –transmission probability in each interaction—and the

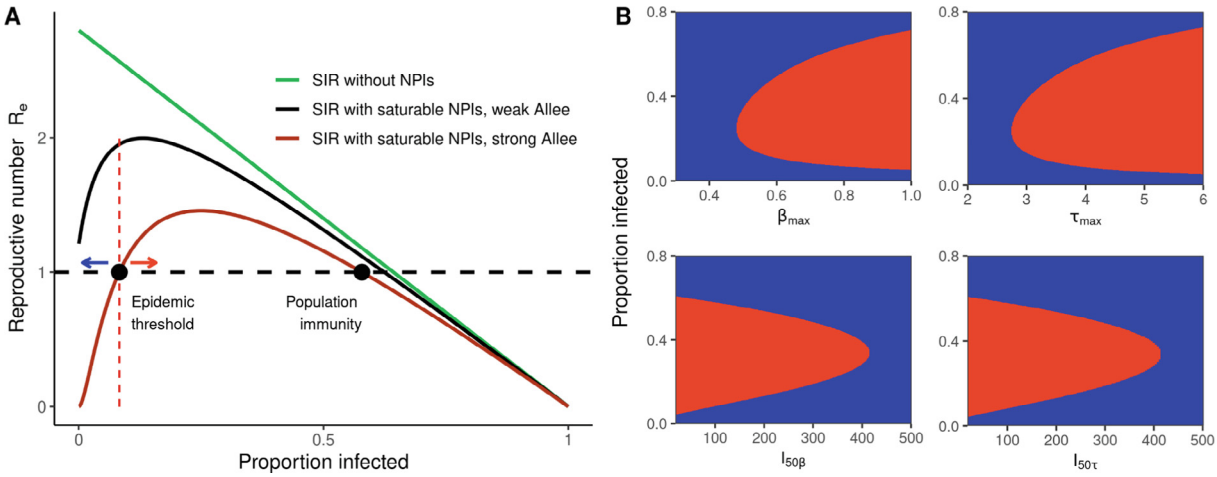

Fig. 2. Saturation processes and disease dynamics. These results are similar to those presented in Fig. 1 but obtained from a general SIR model with a rise in transmission rate (β) and infectious period (τ) with I. **(A)** Effective reproduction number as a function of the proportion of the population infected $R_e(I)$. For the green line (SIR without NPIs), β was fixed to β_{max} and τ was fixed to τ_{max}. For the red line (model with saturable NPIs inducing strong Allee effect), the model parameters were: $\beta_{max} = 0.7$, $\tau_{max} = 4$, $I_{50,\beta} = 100$, $I_{50,\tau} = 100$, and $\beta_0 = \tau_0 = 0$. For the black line (model with staurable NPIs inducing a weak Allee effect), the same parameters as for the red line were used, except for the modifications of $\beta_0 = 0.4$ and $\tau_0 = 3$. Arrows highlight the expected trend in infection numbers around the infection threshold. (**B**) The alternative epidemic states of growth ($R_e(I) > 1$, red) or containment ($R_e(I) < 1$, blue) are determined by both the proportion of the infected population (vertical axis) and the transmission and infectious period parameters. These parameters capture the saturation in contact tracing with the rise in infection number ($I_{50,\beta}$, $I_{50,\tau}$) and the strength of other NPIs (β_{max}, τ_{max}). Parameters used were the same as for the strong Allee effect in panel A, with exception of the parameter varied in the horizontal axis.

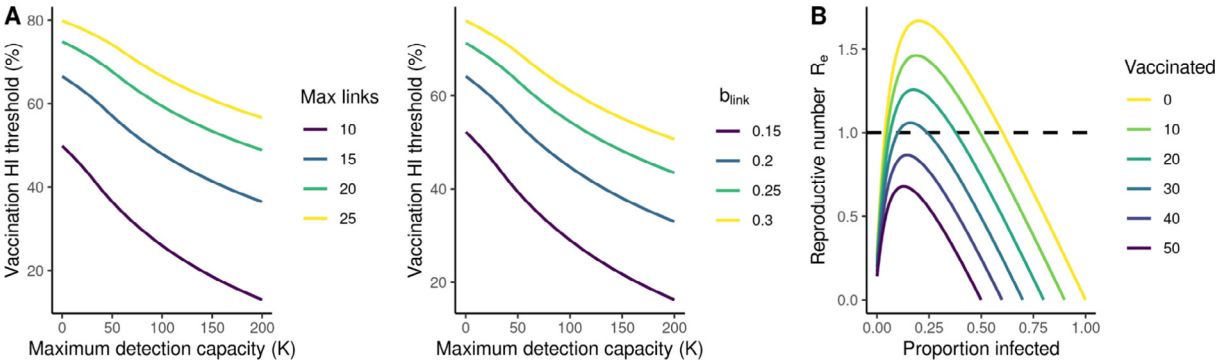

Fig. 3. Interaction between immunization (vaccination and recovered population fraction) levels and contact tracing for different strengths of social interactions and transmission barriers. **(A)** Vaccinated threshold for population immunity as a function of the contact tracing capacity (horizontal axis) and for different levels of social interactions (left) and of hygienic measures (right), as indicated by the line colors. The estimates were obtained using the same model as for the strong Allee effect in Fig. 1A, with the same model parameters, except for those that are varied in the plots. **(B)** Relation between reproductive value R_e and proportion of infected individuals for different levels of population vaccination assuming a 100% effective vaccine. Reduction in vaccine effectiveness has the same effect as vaccination in a reduced fraction of the population. Estimates are obtained using the same parameter values as in Fig. 1A for the strong Allee effect.

strength of the contact tracing system by the parameters *K and* N_{calls}—maximum number of cases that could be detected and calls alerts in a day respectively. As it becomes evident in Fig. 1B, the effect of contact tracing capacities on disease dynamics is contingent to the strength of the other interventions. Models oriented to forecast epidemic dynamics in alternative scenarios and guide management strategies may have to consider the Allee effect to properly capture the mechanisms that govern disease trajectories (e.g. model 2).

Models may inform about the expected epidemic dynamic and the potential performance of alternative containment strategies (Bubar et al., 2021; Grantz et al. 2021; Moore et al., 2021; Yang et al., 2021) but are frequently limited by the sparsity of data (Fitzpatrick and Galvani, 2021). In this context, models capturing basic mechanisms could be particularly important to provide a general understanding of the epidemic dynamics and intervention consequences (Fitzpatrick et al., 2019). On one hand, the two models herein considered provide general insights about the mechanisms determining epidemic dynamics when contact tracing, other NPIs, and vaccination are involved. In particular, the emergence of a positive feedback at low numbers may have large dynamic consequences but it was not included in the SIR and logistic models widely used for the analysis of COVID-19 dynamics. The dependence of infection or recovery rates of the infection number is probably a hypothesis that has to be included when epidemiological models are fitted to observed dynamics; which may significantly enhance the descriptive and forecasting potential of models. On the other hand, the first model considered the basic mechanisms connecting tracing capacities with its saturation and the Allee effect and the second model considered the incorporation of this phenomenon in general SIR models--or its variants. These two models do not demand large amounts of information and may be parametrized with data that is frequently available. When tracing systems are implemented, the information required to parametrize our mechanistic model (Eq. (1)) is typically recorded, and may be used to fit this model or alternative formulations adapted to specific scenarios. Similarly, in the SIR model, the relationship between infection number and the rates of disease

transmission and case isolation can be empirically estimated by fitting the SIR model with saturation (equation (2)) to epidemic data. However, it should be highlighted that other nonlinear functions or non monotonic functions could better describe the empirical relationship between transmission (β) and recovery (τ) rates and the infection number and should be also considered. For example, the balance between saturation of containment capacities with the increase in effectiveness in the detection of infected individuals may determine more complex nonlinear relationships--e.g. U-shaped or humped. Both their suitability in phenomenological models are the proximal mechanisms involved may be a matter of further theoretical and empirical attention.

4.1. Hysteretic behavior of epidemics

Our results emphasize the importance of timing in NPIs deployment (Pei et al., 2020). Interventions with capacity for epidemic containment at low numbers, if implemented after the disease surpassed the threshold, will likely fail (Fig. 4, points *i* and *iv*) (Alonso et al., 2019; Chowell and Nishiura, 2014; Hellewell et al., 2020). Similarly, once a containment scenario is achieved through strong measures, the relaxation of NPIs and contact tracing has to be done in attention to the epidemic threshold in order to avoid outbreak resurgence (Fig. 4, points *i -> v*). In this context, early warning indicators of approaching these tipping points become crucial. For example, when the disease is contained, the fraction of reported infections with no epidemiological link (not detected by the tracing system) and the time between individual exposure and quarantine should decrease through time (Fig. A.2). A systematic increase in these indicators may be an adequate early warning signal that containment could be compromised. It should be noted that the NPIs, as modelled here, show diminishing returns (Gros et al., 2021; Gross et al., 2006). This means that the effect of distancing, transmission barriers and contact tracing on R_e increases less than proportional to the strength of the interventions. A consequence of diminishing returns is that at low infection numbers a single intervention may push the R_e below 1, but at high infection numbers, strengthening the intervention will produce a proportionally lower effect on the containment of the disease. However, combining alternative interventions may operate synergistically in reducing R_e. In our SIR model, the effect of interventions is represented by the functional relationship between number of infections and the recovery and transmission rates. Effective and combined interventions will saturate at larger infection numbers, raising the outbreak threshold, and consequently, improving the conditions for disease containment.

The Allee effect may also interact with stochasticity and external forcing in the course of the epidemics. The role of stochasticity and the Allee effect have been addressed in biological invasions (Taylor and Hastings, 2005). In the context of epidemics, super-spreading events are considered as main drivers of disease dynamics at low numbers (Lloyd-Smith et al., 2005; Zhang et al., 2020). Our results suggest that these infection pulses may have qualitatively different effects when the Allee effect is involved. Indeed, a super-spreading events may determine the surpassing of the infection threshold, I^*, moving the disease into the outbreak zone, with subsequent exponential increase in infections. Similarly, external forces such as transmission barriers or variation in the number of social links may induce changes in the relationship between the effective reproduction number and the fraction of infected individuals (Figs. 1-3). As a consequence, the effect of variation in mobility or face mask usage on R_e depends on the infection state, determining that their correlation--or lack of it—at some level of infection may not directly extrapolate to other infection levels (Royama, 1992). In this sense, the observed variability in the correlation between R_e and mobility at different infection levels could be related to real changes in their association at low numbers and not only to changes in report quality (e.g. Leung et al., 2021). Similarly, populations affected by a correlated external forcing--as changes in mobility--tend to synchronize their dynamics (Moran effect sensu Royama (Royama, 1992; Royama, 2021)), a scenario in which the Allee effect may promote the simultaneous control of the outbreaks or enable global resurgence. However, the Allee effect can also determine a spatial mosaic in which some populations are over and others under the infection threshold, stabilizing regional dynamics by means of preventing the spatial homogenization (Taylor and Hastings, 2005). This could be related with the stabilization and persistence of disease dynamics at low numbers observed in COVID and other diseases. These phenomena should not be ignored when considering strategies for controlling COVID-19, such as the coordinated implementation of measures among countries and regions (Ruktanonchai et al., 2020).

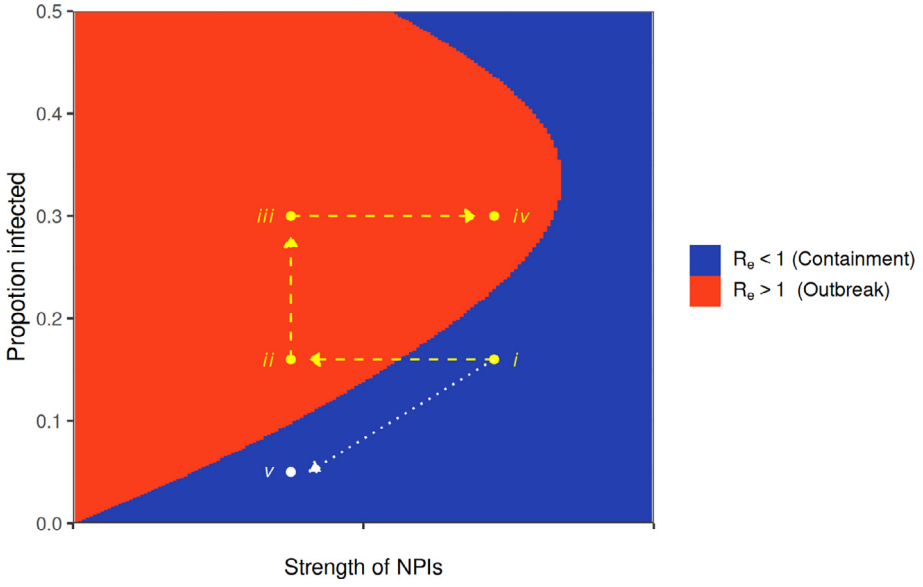

Fig. 4. Relaxation strategies of NPIs and epidemic containment. In trajectory $i \rightarrow ii \rightarrow iii \rightarrow iv$ an abrupt relaxation surpasses the epidemic threshold provoking an increase in infections. Return to previous strength of NPIs fails to contain the outbreak. In trajectory $i \rightarrow v$ the gradual relaxation of NPIs follows the decrease in the infected population keeping epidemic under control.

4.2. NPIs and vaccination synergistic effect on reaching herd immunity

Understanding the interaction between vaccinations and NPIs together with the relaxation of tracing systems (TETRIS) is a main issue in Covid-19 management worldwide (Fitzpatrick and Galvani, 2021; Moore et al., 2021; Yang et al., 2021). One striking result of our models is the impact that NPIs, particularly contact tracing, and the induced Allee effect, may have on the herd immunity threshold. In Eq. (1), vaccination reduces the parameter $P_{susceptible}$, proportionally reducing the expected R_e for each value of I (Fig. 3). Vaccination operates as an external forcing that induces a proportional change in R_e for each value of infections, that is, in absolute values it is larger for larger values of R_e. In population dynamics, this kind of effect of an exogenous variable--vaccination or recovery immunity in this case--is known as a non-linear translation because it changes the shape of the R_e – Infection relationship (Royama, 1992). This improves conditions for reaching a R_e <1 with vaccination (Fig. 3). This is particularly relevant because combining NPIs with vaccination may contain the epidemic at much lower levels of immunization (see also Moore et al., 2021; Yang et al., 2021). This also implies that herd immunity could be attained in shorter times than those required with strategies exclusively based on vaccination. Finally, this interaction between vaccinations and NPIs determines that variations in NPIs strength, or in the combination of containment strategies, among regions may produce variation in the vaccination level required to attain herd immunity.

4.3. General remarks

In this work we focused on the saturation of contact tracing capacities, however, other elements of the NPIs strategy may also saturate with the number of infections. The effect of face masks, hygiene measures, and physical distance is expected to decrease with a higher pathogen load in the environment (Prather et al., 2020). Indeed, for COVID-19 it was reported that among non-household contacts the infection odds ratio when an individual is exposed to more than one case is close to four (Ng et al., 2020). The healthcare system's saturation delays case isolation, extending the infectious period, and may produce shortages of protective material, increasing transmission rate (Abdelrazec et al., 2016; Chowell and Nishiura, 2014). It is also true that awareness-driven individual behaviour or reactive management strategies may induce the opposite phenomenon, increasing the contact tracing and other NPIs performance with the rise in infections (Leung et al., 2021; Lewis, 2020; Weitz et al., 2020). In addition, the efficiency of tracers in "capturing" infected individuals may increase with the infection numbers. At low numbers contact tracing efforts result in identifying non-infected individuals. However, as the infectiousness burden goes up in the community, the probability a contact is truly infected will also increase; this means that numbers of contagions stopped by the tracing system could be particularly high. Even if tracers are not enough to revert the epidemic growth, they may have a large role in the reduction of new cases, thus in deaths and in the occupation of hospital facilities. This decrease or increase in intervention effectiveness in response to the state of the epidemic may generate positive and negative feedbacks in disease growth rate (Berryman, 1999; Bjørnstad, 2018; Elkington et al., 1995; Royama, 1992; Royama, 2021). In these cases, NPIs operate as a reactive environment that may revert disease growth rate but that may also induce cyclic dynamics, particularly at low infection numbers when they have a strong effect on disease transmission (Berryman, 1999; Lima, 2009; Royama, 1992; Royama, 2021; Turchin, 2003; Weitz et al., 2020). Large amplitudes in induced cycles may provide the conditions for surpassing the infection threshold and the epidemic outbreak, representing a phenomenon that should be better understood.

In spite of the large attention to the Allee effect in Ecology, its detection on real population dynamics is recognized as a significant challenge (Johnson et al., 2006; Tobin et al., 2007). Accelerations with a qualitative change in disease growth rate were frequently observed in COVID-19 epidemics (e.g. Carroll et al., 2020; Kang et al., 2020; Laxminarayan et al., 2020). An Allee effect induced by the saturation of contact tracing capacities or other NPIs may explain some of these abrupt transitions in COVID-19 spreading. However, temporal change in intervention strength (Li et al., 2020), awareness-driven behavior (Weitz et al., 2020), change in testing strategy (Omori et al., 2020) and aggregation of local dynamics in a regional dynamic (Kang et al., 2020) can also determine the observation of abrupt transitions in the disease growth rate. As is the case for population dynamics studies, the quantification of the Allee effect in disease dynamics may require novel approaches, which could include the interaction with additional mechanisms together with idiosyncratic features and information from each particular system (Johnson et al., 2006; Tobin et al., 2007).

Amidst an ongoing worldwide outbreak of COVID-19, studies connecting contact tracing and other NPIs with disease dynamics are all the more needed (Block et al., 2020; Haug et al., 2020; Hsiang et al., 2020; Maier and Brockmann, 2020; Moore et al., 2021; Peak et al., 2017; Peak et al., 2020; Ruktanonchai et al., 2020; Walker et al., 2020a; Yang et al., 2021). Our results link NPIs in general, and contact tracing in particular, with the substantial knowledge built around the Allee effect and tipping points in ecology (Courchamp et al., 1999; Scheffer, 2009; Taylor and Hastings, 2005), and also with previous studies that related the saturation of NPIs, reactive individual behavior, and positive feedbacks with disease dynamics (Abdelrazec et al., 2016; Alonso et al., 2019; Chowell and Nishiura, 2014; Funk et al., 2010; Gross et al., 2006; Gumel, 2012). The recognition of a contact tracing-induced Allee effect, its interaction with vaccination and the existence of tipping points contributes to the understanding of several features of disease dynamics and its response to containment interventions. It becomes clear that this result opens up interesting questions from both the theoretical and the applied realms. This knowledge may be of relevance for explaining the dynamics of COVID-19 and other diseases in different regions and, more importantly, as input for guiding the use of NPIs relaxation strategies, vaccination campaigns, and its combination for the management of epidemic outbreaks.

Authors thank comments from GUIAD and GACH. This study was significantly improved from comments of Nils Stenseth, Andrew Dobson, Pablo Marquet, and Marten Scheffer, who together with four anonymous reviewers made significant contributions, indicating the main strength and limitations of the Allee effect for explaining COVID-19 dynamics, proposing alternative mechanisms and ways to clarify the presentation of models.

Declaration of Competing Interest

The authors declare that they have no known competing financial interests or personal relationships that could have appeared to influence the work reported in this paper.

Funding

MA. thanks CSIC groups-657725. This work was partially supported by CSIC-UdelaR, PEDECIBA and ANII. Centro interdisciplinario en Ciencia de Datos y Aprendizaje Automático (CICADA), UdelaR.

Appendix A

Figs. A1 and A2.

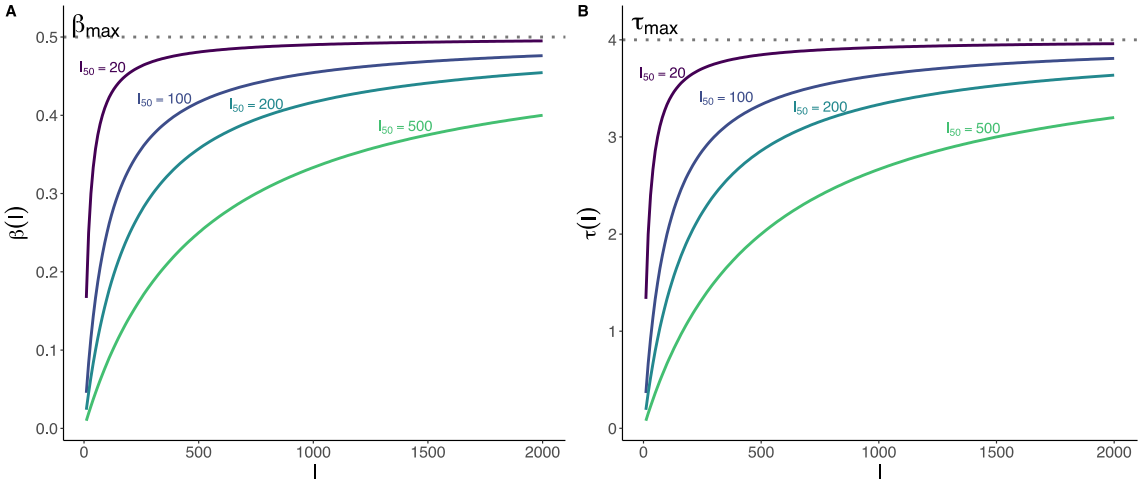

Fig. A1. Relationship between transmission rate $\beta(I)$ and infection period $\tau(I)$ with the number of infected individuals in the SIR model with saturation of tracing capacities analyzed in the article. Both parameters grow with the number of infected individuals I, following the saturating functions $\beta_t(I) = \beta_0+(\beta_{max}-\beta_0)\cdot I(t)/(I_{50,\beta} + I(t))$ and $\tau_t(I) = \tau_0+(\tau_{max}-\tau_0)\cdot I(t)/(I_{50,\tau} + I(t))$ respectively. The parameters $I_{50,\beta}$ and $I_{50,\tau}$ are the number of infection numbers at which transmission rate and infection period attain half of its maximum values β_{max} and τ_{max}. β_0 and τ_0 represent the smaller transmission rate and infection period, which are attained at the lower level of infection. The saturation parameters $I_{50,\beta}$ and $I_{50,\tau}$ summarize the different components of the tracing strategy: the better performance of a tracing system is, the larger the $I_{50,\beta}$ and $I_{50,\tau}$ values will be. In this example, $\beta_0 = \tau_0 = 0$, $\beta_{max} = 0.5$ and $\tau_{max} = 4$.

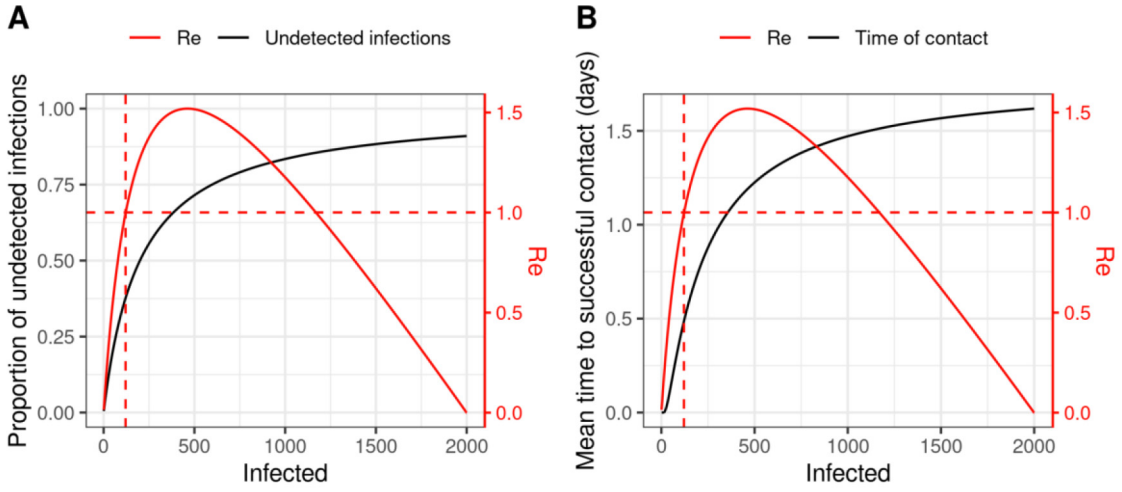

Fig. A2. Trends in the proportion of infections without epidemiological link (**A**) and on the time between case detection and isolation (**B**) with the rise of infection number. The horizontal dashed lines indicate Re = 1 and the vertical dashed line the infection number at which Re suprass 1 determining the infection outbreak. The interceptions of these vertical dashed lines and the black lines indicate the proportion of infections without epidemiological link (**A**) and the time to isolation (**B**) at which containment capacities are surpassed by the infection number. The parameters used in the simulation are the same as in Fig. 1 in the main text: For the red line with strong NPI-Allee effect, the model parameters are P_{find} = 0.1, N_{Calls} = 800, b_{link} = 0.2, L_{Max} = 14, K = 200 and I_{50} = 200 and N = 2000.

References

Abdelrazec, A., Bélair, J., Shan, C., Zhu, H., 2016. Modeling the spread and control of dengue with limited public health resources. Mathematical biosciences 271, 136–145.

Alonso, D., Dobson, A., Pascual, M., 2019. Critical transitions in malaria transmission models are consistently generated by superinfection. Philosophical Transactions of the Royal Society B 374, 20180275.

Berryman, A.A., 1999. Principles of Population Dynamics and Their Application. Stanley Thornes, Cheltenham, U.K..

Bjørnstad, O.N., 2018. Epidemics: models and data using R. Springer.

Block, P., Hoffman, M., Raabe, I.J., Dowd, J.B., Rahal, C., Kashyap, R., Mills, M.C., 2020. Social network-based distancing strategies to flatten the COVID-19 curve in a post-lockdown world. Nature Human Behaviour, 1–9.

Bubar, K.M., Reinholt, K., Kissler, S.M., Lipsitch, M., Cobey, S., Grad, Y.H., Larremore, D.B., 2021. Model-informed COVID-19 vaccine prioritization strategies by age and serostatus. Science 371, 916–921.

Carroll, C., Bhattacharjee, S., Chen, Y., Dubey, P., Fan, J., Gajardo, Á., Zhou, X., Müller, H.G., Wang, J.L., 2020. Time dynamics of COVID-19. Scientific reports 10, 1–14.

Chowell, G., Nishiura, H., 2014. Transmission dynamics and control of Ebola virus disease (EVD): a review. BMC medicine 12, 196.

Chowell, G., Tariq, A., Hyman, J.M., 2019. A novel sub-epidemic modeling framework for short-term forecasting epidemic waves. BMC medicine 17, 164.

Courchamp, F., Clutton-Brock, T., Grenfell, B., 1999. Inverse density dependence and the Allee effect. Trends in ecology & evolution 14, 405–410.

Dehning, J., Zierenberg, J., Spitzner, F.P., Wibral, M., Neto, J.P., Wilczek, M., Priesemann, V., 2020. Inferring change points in the spread of COVID-19 reveals the effectiveness of interventions. Science.

Elkington, J., Begon, M., Godfray, C., Hall, A., de Jong, M., Gascoyne, S., Bowers, R., Briggs, C., Laurenson, K., Hails, R., 1995. Microparasite group report: persistence of microparasites in natural populations. Ecology of infectious diseases in natural populations. Cambridge University Press, Cambridge, pp. 123–143.

Ferretti, L., Wymant, C., Kendall, M., Zhao, L., Nurtay, A., Abeler-Dörner, L., Parker, M., Bonsall, D., Fraser, C., 2020. Quantifying SARS-CoV-2 transmission suggests epidemic control with digital contact tracing. Science 368.

Fitzpatrick, M.C., Bauch, C.T., Townsend, J.P., Galvani, A.P., 2019. Modelling microbial infection to address global health challenges. Nature microbiology 4, 1612–1619.

Fitzpatrick, M.C., Galvani, A.P., 2021. Optimizing age-specific vaccination. Science 371, 890–891.
Flaxman, S., Mishra, S., Gandy, A., Unwin, H.J.T., Mellan, T.A., Coupland, H., Whittaker, C., Zhu, H., Berah, T., Eaton, J.W., 2020. Estimating the effects of non-pharmaceutical interventions on COVID-19 in Europe. Nature, 1–8.
Funk, S., Salathé, M., Jansen, V.A., 2010. Modelling the influence of human behaviour on the spread of infectious diseases: a review. Journal of the Royal Society Interface 7, 1247–1256.
Gotelli, N.J., 2008. A primer of ecology. Sinauer Associates, Sunderland.
Grantz, K.H., Lee, E.C., D'Agostino McGowan, L., Lee, K.H., Metcalf, C.J.E., Gurley, E.S., Lessler, J., 2021. Maximizing and evaluating the impact of test-trace-isolate programs: A modeling study. *PLoS medicine* 18, (4) e1003585.
Gros, C., Valenti, R., Schneider, L., Valenti, K., Gros, D., 2021. Containment efficiency and control strategies for the Corona pandemic costs. Scientific reports 11, 1–13.
Gross, T., D'Lima, C.J.D., Blasius, B., 2006. Epidemic dynamics on an adaptive network. Physical review letters 96, 208701.
Gumel, A., 2012. Causes of backward bifurcations in some epidemiological models. Journal of Mathematical Analysis and Applications 395, 355–365.
Haug, N., Geyrhofer, L., Londei, A., Dervic, E., Desvars-Larrive, A., Loreto, V., Pinior, B., Thurner, S., Klimek, P., 2020. Ranking the effectiveness of worldwide COVID-19 government interventions. Nature Human Behaviour, 1–10.
He, X., Lau, E.H., Wu, P., Deng, X., Wang, J., Hao, X., Lau, Y.C., Wong, J.Y., Guan, Y., Tan, X., 2020. Temporal dynamics in viral shedding and transmissibility of COVID-19. Nature medicine 26, 672–675.
Hellewell, J., Abbott, S., Gimma, A., Bosse, N.I., Jarvis, C.I., Russell, T.W., Munday, J.D., Kucharski, A.J., Edmunds, W.J., Sun, F., 2020. Feasibility of controlling COVID-19 outbreaks by isolation of cases and contacts. The Lancet Global Health.
Hsiang, S., Allen, D., Annan-Phan, S., Bell, K., Bolliger, I., Chong, T., Druckenmiller, H., Huang, L.Y., Hultgren, A., Krasovich, E., Lau, P., Lee, J., Rolf, E., Tseng, J., Wu, T., 2020. The effect of large-scale anti-contagion policies on the COVID-19 pandemic. Nature. https://doi.org/10.1038/s41586-020-2404-8.
Johnson, D. M., Liebhold, A. M., Tobin, P. C., Bjørnstad, O. N., 2006. Allee effects and pulsed invasion by the gypsy moth. Nature, 361-363, doi:doi:10.1038/nature05242.
Kang, D., Choi, H., Kim, J.H., Choi, J., 2020. Spatial epidemic dynamics of the COVID-19 outbreak in China. International Journal of Infectious Diseases 94, 96–102.
Keeling, M.J., Rohani, P., 2011. Modeling infectious diseases in humans and animals. Princeton University Press.
Klinkenberg, D., Fraser, C., Heesterbeek, H., 2006. The effectiveness of contact tracing in emerging epidemics. PloS one 1, e12.
Laxminarayan, R., Wahl, B., Dudala, S.R., Gopal, K., Neelima, S., Reddy, K.J., Radhakrishnan, J., Lewnard, J.A., 2020. Epidemiology and transmission dynamics of COVID-19 in two Indian states. Science 370, 691–697.
Lee, C.K., Song, H.J., Bendle, L.J., Kim, M.J., Han, H., 2012. The impact of non-pharmaceutical interventions for 2009 H1N1 influenza on travel intentions: A model of goal-directed behavior. Tourism Management 33, 89–99.
Leung, K., Wu, J.T., Leung, G.M., 2021. Real-time tracking and prediction of COVID-19 infection using digital proxies of population mobility and mixing. Nature communications 12, 1–8.
Lewis, D., 2020. Why many countries failed at COVID contact-tracing-but some got it right. Nature 588, 384–387.
Li, R., Pei, S., Chen, B., Song, Y., Zhang, T., Yang, W., Shaman, J., 2020. Substantial undocumented infection facilitates the rapid dissemination of novel coronavirus (SARS-CoV-2). Science 368, 489–493.
Lima, M., 2009. A link between the North Atlantic Oscillation and measles dynamics during the vaccination period in England and Wales. Ecology letters 12, 302–314.
Lloyd-Smith, J.O., Schreiber, S.J., Kopp, P.E., Getz, W.M., 2005. Superspreading and the effect of individual variation on disease emergence. Nature 438, 355–359.
Maier, B.F., Brockmann, D., 2020. Effective containment explains subexponential growth in recent confirmed COVID-19 cases in China. Science 368, 742–746.
Markel, H., Lipman, H.B., Navarro, J.A., Sloan, A., Michalsen, J.R., Stern, A.M., Cetron, M.S., 2007. Nonpharmaceutical interventions implemented by US cities during the 1918–1919 influenza pandemic. Jama 298, 644–654.
Moore, S., Hill, E.M., Tildesley, M.J., Dyson, L., Keeling, M.J., 2021. Vaccination and non-pharmaceutical interventions for COVID-19: a mathematical modelling study. The Lancet Infectious Diseases 21, 793–802.
Ng, O.T., Marimuthu, K., Koh, V., Pang, J., Linn, K.Z., Sun, J., De Wang, L., Chia, W.N., Tiu, C., Chan, M., 2020. SARS-CoV-2 seroprevalence and transmission risk factors among high-risk close contacts: a retrospective cohort study. The Lancet Infectious Diseases 21 (3), 333–343.
Omori, R., Mizumoto, K., Chowell, G., 2020. Changes in testing rates could mask the novel coronavirus disease (COVID-19) growth rate. International Journal of Infectious Diseases 94, 116–118.
Peak, C.M., Childs, L.M., Grad, Y.H., Buckee, C.O., 2017. Comparing nonpharmaceutical interventions for containing emerging epidemics. Proceedings of the National Academy of Sciences 114, 4023–4028.
Peak, C.M., Kahn, R., Grad, Y.H., Childs, L.M., Li, R., Lipsitch, M., Buckee, C.O., 2020. Individual quarantine versus active monitoring of contacts for the mitigation of COVID-19: a modelling study. The Lancet Infectious Diseases 20, 1025–1033.
Pei, S., Kandula, S., Shaman, J., 2020. Differential effects of intervention timing on COVID-19 spread in the United States. Science advances 6, eabd6370.
Prather, K.A., Wang, C.C., Schooley, R.T., 2020. Reducing transmission of SARS-CoV-2. Science 368, 1422–1424.
Roosa, K., Lee, Y., Luo, R., Kirpich, A., Rothenberg, R., Hyman, J., Yan, P., Chowell, G., 2020. Real-time forecasts of the COVID-19 epidemic in China from February 5th to February 24th, 2020. Infectious Disease Modelling 5, 256–263.
Royama, T., 1992. Analytical Population Dynamics. Chapman & Hall, London.
Royama, T., 2021. Animal Population Ecology: An Analytical Approach. Cambridge University Press.
Ruktanonchai, N.W., Floyd, J., Lai, S., Ruktanonchai, C.W., Sadilek, A., Rente-Lourenco, P., Ben, X., Carioli, A., Gwinn, J., Steele, J., 2020. Assessing the impact of coordinated COVID-19 exit strategies across Europe. Science 369, 1465–1470.
Scheffer, M., 2009. Critical Transitions in Nature and Society. Princeton University Press, Princeton.
Siegenfeld, A.F., Taleb, N.N., Bar-Yam, Y., 2020. Opinion: What models can and cannot tell us about COVID-19. Proceedings of the National Academy of Sciences 117, 16092–16095.
Taylor, C.M., Hastings, A., 2005. Allee effects in biological invasions. Ecology Letters 8, 895–908.
Tobin, P.C., Whitmire, S.L., Johnson, D.M., Bjørnstad, O.N., Liebhold, A.M., 2007. Invasion speed is affected by geographical variation in the strength of Allee effects. Ecology Letters 10, 36–43. https://doi.org/10.1111/j.1461-0248.2006.00991.x.
Turchin, P., 2003. Complex population Dynamics: a theoretical/empirical synthesis. Princeton University Press, New Jersey.
Viboud, C., Simonsen, L., Chowell, G., 2016. A generalized-growth model to characterize the early ascending phase of infectious disease outbreaks. Epidemics 15, 27–37.
Walker, P., Whittaker, C., Watson, O., Baguelin, M., Ainslie, K., Bhatia, S., Bhatt, S., Boonyasiri, A., Boyd, O., Cattarino, L., 2020a. Report 12: The global impact of COVID-19 and strategies for mitigation and suppression.
Walker, P.G., Whittaker, C., Watson, O.J., Baguelin, M., Winskill, P., Hamlet, A., Djafaara, B.A., Cucunubá, Z., Mesa, D.O., Green, W., 2020b. The impact of COVID-19 and strategies for mitigation and suppression in low-and middle-income countries. Science 369, 413–422.
Weitz, J.S., Park, S.W., Eksin, C., Dushoff, J., 2020. Awareness-driven behavior changes can shift the shape of epidemics away from peaks and toward plateaus, shoulders, and oscillations. Proceedings of the National Academy of Sciences 117, 32764–32771.
Wu, K., Darcet, D., Wang, Q., Sornette, D., 2020. Generalized logistic growth modeling of the COVID-19 outbreak in 29 provinces in China and in the rest of the world. arXiv preprint arXiv:2003.05681.
Yang, J., Marziano, V., Deng, X., Guzzetta, G., Zhang, J., Trentini, F., Cai, J., Poletti, P., Zheng, W., Wang, W., Wu, Q., Zhao, Z., Dong, K., Zhong, G., Viboud, C., Merler, S., Ajelli, M., Yu, H., 2021. Despite vaccination, China needs non-pharmaceutical interventions to prevent widespread outbreaks of COVID-19 in 2021. Nature Human Behaviour. https://doi.org/10.1038/s41562-021-01155-z.
Zhang, Y., Li, Y., Wang, L., Li, M., Zhou, X., 2020. Evaluating transmission heterogeneity and super-spreading event of COVID-19 in a metropolis of China. International Journal of Environmental Research and Public Health 17, 3705.